Bottom Drag Coefficient on a Shallow Barrier Reef

Damien Sous, Samantha Maticka, Samuel Meulé, Frédéric Bouchette

Bottom drag coefficient on a shallow barrier reef

Damien Sous[1,2], **Samantha Maticka** [3], **Samuel Meulé** [4], **Frédéric Bouchette** [3]

[1]Université de Toulon, Aix Marseille Université, CNRS, IRD, Mediterranean Institute of Oceanography (MIO), La Garde, France
[2]Universite de Pau et des Pays de l'Adour, E2S UPPA, SIAME, Anglet, France
[3]GEOSCIENCES-Montpellier, Univ Montpellier, CNRS, Montpellier, France
[4]Aix Marseille University, CNRS, IRD, INRAE, Coll France, CEREGE, Aix-en-Provence, France

Key Points:

- Field estimates of bottom drag coefficient over a shallow rough coral barrier reef using a bulk momentum balance approach
- Drag coefficients are dependent on the local depth and colony structure, and well predicted by a log dependency
- The recovered data allows for a discussion of the connection between hydrodynamic roughness scale and high resolution seabed topography

Corresponding author: Damien Sous, sous@univ-tln.fr

Abstract

The present paper reports of a field experiment over a shallow, roughness-varying barrier reef at Maupiti island, French Polynesia. The depth-averaged momentum balance is used to estimate the bottom drag coefficient C_d, which varies from 0.01 to 0.3, with dependence on both depth and reef structure. The depth effect on C_d is well predicted by a log dependency, as used in previous laboratory and fields observations. The present results extend the approach to a system with more wave exposure and higher roughness-to-depth ratio. Additionally, the statistical relationship between high-resolution reef topography and hydrodynamical parameters is discussed.

Plain Language Summary

Coral reefs are essential for human societies and ecosystems in many tropical coastlines. Having reliable hydrodynamic models of these systems is important for proper management and engineering applications. Reefs play an important role in sheltering shorelines by attenuating wave energy and slowing currents. Thus, they must be accounted for in the models. However, due to the complexity of coral geometry, there is still no reliable manner to represent or translate the physical observation of corals' geometrical structure to a friction term in the governing equations of the models. Additional representative challenges exist due to the varying importance of friction, depending on the water depth. This paper demonstrates good alignment between a metric of the physical geometry of coral to a frictional parameter used in the governing equation, the momentum balance. Additionally, the depth dependence of our results is described well by a classical equation meant to describe turbulence near a wall, log-layer theory. In total, the results yields good agreement between terms in the momentum balance and aid in the fundamental connection of the physically-observed and the numerically-representation reefs.

1 Introduction

Coral reefs are in decline worldwide, with dramatic consequences for tropical ecosystems and human communities. Anticipating and mitigating the impacts of coral reef degradation requires a comprehensive knowledge of reef hydrodynamics (Monismith, 2007), which in turn strongly affect wave transformation (Hearn, 1999; Lowe et al., 2005; A. Pomeroy et al., 2012; Sous et al., 2019), water residence time (Chevalier et al., 2015; Reid et al., 2020) and sediment transport (A. W. Pomeroy et al., 2017) in reef-lagoon systems.

As emphasized by the review from Davis et al. (2020), coral colonies generally exhibit a spectacular geometric complexity which plays an overwhelming role in the frictional dissipation of water motions in coral reef-lagoon systems. Over the last two decades, significant research efforts have been made to capture the effects of coral reef roughness on both the wave energy and momentum balance equations used in nearshore wave and circulation models (Lowe et al., 2005; Rosman & Hench, 2011; Monismith et al., 2015; A. W. Pomeroy et al., 2017; Lentz et al., 2018; Sous, Dodet, et al., 2020). Of particular importance is the representation of bottom friction processes in the momentum balance, which is often considered in the depth-averaged formulation in shallow nearshore systems to allow for exploration and prediction of the dominant drivers of water levels and current dynamics in reef-lagoon systems. While simple linear functions have been used in early analytical models (Symonds et al., 1995; Hearn, 1999), currently the most common approach is to parameterize the bottom stress as a quadratic function (M. R. Gourlay & Colleter, 2005; Monismith, 2007; Davis et al., 2020), using a dimensionless bottom drag coefficient, C_d as a key parameter. Field studies on coral reef have shown that coral reef C_d are generally at least one order of magnitude larger than their counterparts observed on sandy beaches owing to the

preponderant effect of pressure drag over skin friction drag (Rosman & Hench, 2011). Field-inferred C_d also show a very large spread between sites, measurement methods and C_d definition (Rosman & Hench, 2011). This variability is explained by the variability of natural coral reef systems, the surface wave effects, and by the fact that in such a complex context, local measurements may be affected by specific terrain features (Hench & Rosman, 2013) and therefore may not be representative of the integrated effect of the coral reef on bottom friction (Reidenbach et al., 2006). For large roughness height to depth ratio, the usual framework of drag processes over rough bottoms can be undermined by the additional role of the flow within the coral colony, often called in-canopy flow (Rosman & Hench, 2011; Davis et al., 2020). This emphasizes the importance of the local depth relative to the physical height of coral colonies in frictional processes, which can be parameterized with empirical power-laws of depth (McDonald et al., 2006) or with formulations derived from the turbulent boundary layer theory (A. Pomeroy et al., 2012; Lentz et al., 2017, 2018; Sous, Dodet, et al., 2020). However, it is worth mentioning that, apart from these few latter exceptions, the depth-effect is not systematically explored and field-inferred C_d are often presented as constant for a given site. A pivotal research prospect is to establish a connection between the hydrodynamic parameters describing bottom friction, such as the bottom drag coefficient or other hydrodynamic roughness heights, and the actual geometrical structure of the reef colony (Lowe et al., 2005; Davis & Monismith, 2011; Lentz et al., 2017; Rogers et al., 2018). This remains a fierce challenge, since it requires both a robust characterization of the hydrodynamic parameters related to bottom friction and a fine knowledge of the reef geometry. Aiming to explore this issue in the coral reef context, a specific field site was selected due to (i) an overall high roughness to depth ratio, (ii) a spatially-varying and well partitioned geometrical reef structure that allows for an assessment of geometric variations effect on bottom friction, (iii) a series of high-resolution measurements of the coral colony structure (Sous, Bouchette, et al., 2020), and (iv) a hydrodynamic field campaign designed to provide robust characterization of the bottom drag coefficient. The objectives of the present study are to present and discuss these latter field measurements and to discern the potential relationship between hydrodynamic bottom friction and the actual coral colony topography. A particular focus is given on both depth and reef structure effects on the bottom stress.

2 Experiment

The field site, instrumentation, and data processing methods were chosen and designed to allow for a bulk analysis of bottom friction through the depth-averaged momentum balance equation (Eq. 1).

2.1 Field site and instrumentation

2.1.1 The Maupiti island

Maupiti ("the Stuck Twins") is a diamond-shaped island located in the western part of the Society archipelago in French Polynesia. The study site is a cross-reef transect located in the south-west barrier (Fig. 1A). This living reef barrier is nearly rectilinear, extending over about 5 km from the west motu (emerged land) to the south pass. The cross-shore profile of the selected area appears representative of the nearly uniform reef structure observed over 4 km of this southwestern barrier (Figs. 1A, B).

2.1.2 Bathymetry

A series of high-resolution topo-bathymetric surveys were carried out to characterize the fine geometrical structure of the reef barrier, see (Sous, Bouchette, et al., 2020), and combined with larger scale bathymetry data. Profiles P1 and P2 from Sous

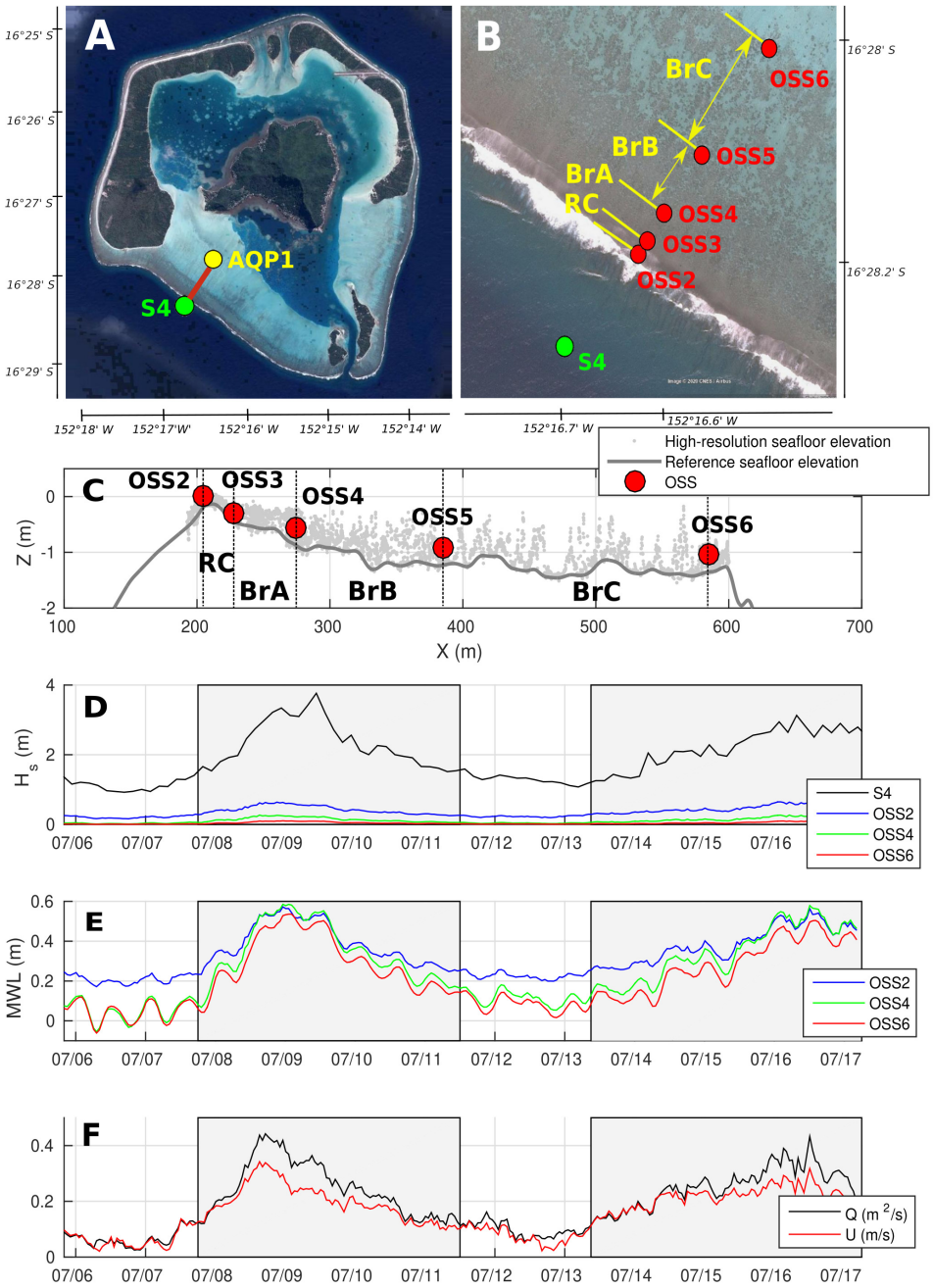

Figure 1. Field site, experimental setup, and meteo-marine conditions. A: satellite view of the Maupiti island with the instrumented transect (red line) extending from S4 to AQP1. B: zoomed satellite view of the instrumented transect with the four selected zones as Reef Crest (RC), Backreef A (BrA), Backreef B (BrB) and Backreef C (BrC). C: cross-shore profile with high-resolution seafloor elevation (P1 and P2 from Sous et al. (Sous, Bouchette, et al., 2020), in grey dots), reference seafloor elevation (solid line) and pressure sensors (red dots). The vertical dashed lines highlight the structural reef zonation. D: SW significant wave heights at S4, OSS2, OSS4, and OSS6. E: Mean Water Level at OSS2, OSS4 and OSS6. F: cross-barrier transport and depth-averaged velocity. The grey patches indicates the periods selected for the analysis of the momentum balance.

et al. (2020), which closely overlap the instrumentation presented here, are combined to provide high-resolution reef topography denoted in grey dots in Figure 1C. The breaking zone extending from the mid-forereef to the reef crest remains inaccessible due to violent wave dynamics.

The definition of the actual seabed is not straightforward in such a complex environment. The approach used here is based on the analysis of the geometrical reef structure proposed by Sous et al. (2020). The high-resolution reef topography is processed with a 7m-wide moving window, corresponding to the fractal breakup observed on reef elevation spectra (Sous, Bouchette, et al., 2020). A statistical threshold is selected to extract the seafloor elevation from the distribution of reef elevation obtained in each moving window. Specifically, the Reference Seafloor Elevation (RSE) used in the momentum balance is defined as the 10-th percentile of the reef elevation. This approach preserves topographical wave-lengths larger than 7 m, which are deemed *bathymetry-related terrain features* (mainly dead substratum), while smaller length-scales associated with living reef colonies are considered *roughness-related terrain features*. An initial discussion of this choice has been proposed by Sous et al. (2020) from geometrical, biological, and reef-history perspectives. Additional hydrodynamic arguments are discussed in the Discussion section (Section 4).

In order to characterize the reef geometry, the reef is divided into four successive zones. Zones were distinguished using a series of statistical metrics, spectral analysis, and/or underwater observations (Sous, Bouchette, et al., 2020). For each zone, we describe the geometry using statistical parameters from the distribution of reef elevation. The zones are highlighted in Figure 1 by vertical dashed lines. Positions along the studied cross-reef transect are defined in a onshore-directed reference starting at isobath -20m.

- The reef crest (RC) is the highest portion of the barrier, extending from $X = 195$ to $X = 225$ m. It is made of small compact coral colonies, typically 20 cm high. This compact, homogeneous structure is related to small values of standard deviation ($\sigma = 0.050$ m) and skewness (-0.37) of reef elevation across the zone.
- The first part of the backreef (BrA), from $X = 225$ to $X = 274$ m, shows a gentle downward slope (-0.6%). While a compact reef structure remains, it is broken by numerous channels up to 50 cm deep. The standard deviation here is $\sigma = 0.19$ m while the skewness is strongly negative (-0.63), tending toward a *d- or δ-type* roughness (Jiménez, 2004; Leonardi et al., 2007).
- The second part of the backreef (BrB), from $X = 274$ to $X = 385$ m, shows a lower downward slope (-0.3%). The reef structure is more open with the presence of higher, larger, and scattered reef elements. This results in a similar standard deviation as Zone A ($\sigma = 0.19$ m) and a weaker, but still negative, skewness (-0.38).
- The last part of the backreef (BrC), from $X = 385$ to $X = 585$ m, is nearly horizontal (average slope -0.023%) and made of spaced out meter-high reef coral mounds on a smooth substratum partly covered by a thin layer of sand (10-30 cm). The standard deviation increases slightly ($\sigma = 0.24$ m), and the skewness shifts to strongly positive value (0.71), revealing the transition toward a *k-type* roughness, i.e. distinct and well spaced roughness elements on a nearly flat bed (Wooding et al., 1973; Jiménez, 2004; Rogers et al., 2018).

2.1.3 Instrumentation

The instrumentation was deployed on a single cross-shore transect (Fig. 1) from July, 5 to 18, 2018. Incoming wave conditions are provided by a S4DW electromagnetic current meter deployed on the forereef, in 10.5 m depth, recording 20-min bursts of data every 3h. Five bottom-mounted pressure sensors (OSSI-010-003®, 10Hz

sampling frequency), namely OSS2 to OSS6, were deployed across the reef barrier to monitor wave and mean water levels. OSS2 was located at the top of the reef crest. Other sensors were placed at the boundaries of the three backreef zones, such that sensor pairs OSS2-OSS3, OSS3-OSS4, OSS4-OSS5, and OSS5-OSS6 allow for monitoring the four barrier portions RC, BrA, BrB, and BrC, respectively. The effect of dynamic pressure was minimized by placing the sensors in reef grooves with a nearly alongshore direction. To capture transport, an acoustic Doppler profiler AQP1 (Nortek sidelooking Aquadopp®) was bottom moored in the lagoon, 500m beyond the barrier. The velocity profiles were recorded every 15 s over a 10-cm cell in 1.5 to 2 m water depth. The measured velocities were projected onto the reef barrier axes to obtain the cross and along-reef components.

2.2 Data processing

2.2.1 Waves

Free surface energy spectra were computed over 60-min bursts subdivided from the continuous record. For each pressure sensor, a discrete Fourier transform was computed without any windowing. The resulting bottom pressure spectra were then converted into free surface elevation spectra using linear wave theory.

2.2.2 Mean water levels and vertical positioning

Particular attention was given to the mean water level measurement in order to improve the accuracy of momentum flux estimates with respect to previous field work (Sous, Bouchette, et al., 2020). Each pressure sensor was repeatedly positioned by Real Time Kinematic Differential Global Navigation Satellite System (DGNSS-RTK). The overall uncertainty is similar to the one estimated during high-resolution topography measurements performed by (Sous, Bouchette, et al., 2020), approximately 3 and 15 cm in vertical and horizontal positioning, respectively. The mean water levels were computed from the continuous records subdivided in 60-min bursts. All pressure measurements were corrected using a 3-point calibration carried out ashore just before deployment and after retrieval, and the atmospheric pressure measured ashore.

2.2.3 Momentum terms calculation

Under the assumption of purely cross-reef, steady, alongshore-uniform flow averaged over many wave cycles, the depth-averaged momentum balance can be written (Sous, Dodet, et al., 2020)

$$\underbrace{g\rho\frac{\partial\bar{\eta}}{\partial x}}_{M_s} = -\underbrace{\frac{1}{(\bar{\eta}+h)}\frac{\partial S_{xx}}{\partial x}}_{M_r} - \underbrace{\frac{1}{(\bar{\eta}+h)}\bar{\tau_b}}_{C_d M_f} \qquad \left[N.m^{-3}\right] \tag{1}$$

where g is the gravitational acceleration, ρ the water density, $\bar{\eta}$ the wave setup, h the still water depth, S_{xx} the radiation stress, and τ_b the bed shear stress. The three terms in Equation 1 will be referred to as Slope (M_s), Radiation (M_r) and Friction (M_f) terms. Note that the total friction momentum flux has been written as the product $C_d M_f$ in order to easily extract C_d, the bottom drag coefficient, through the comparison of the three momentum fluxes. The contribution of advection flux in Equation 1 is assumed to be negligible from the reef crest owing to moderate variations of depth (Symonds et al., 1995; Hearn, 1999; M. Gourlay, 1996; Buckley et al., 2015; Sous, Dodet, et al., 2020). Following the approach of Sous et al. (2020), depth-averaged fluxes are estimated between each successive sensor pair over continuous records subdivided into 60-min bursts. The total water depth ($\bar{\eta} + h$) used for the

calculation in Radiation and Friction terms is taken as the mean water depth between two adjacent sensors.

Slope term

The Slope term $M_s = g\rho\frac{\partial\bar{\eta}}{\partial x}$ is computed using the mean water level at each sensor. A positive Slope term at a given location corresponds to a locally positive mean surface slope in a shoreward direction. Uncertainties in the Slope term computation are mostly related to the accuracy in vertical positioning and sensors distance. Considering typical ranges of setup and horizontal distance of $0.2 \pm 0.015\,m$ and $100 \pm 0.075\,m$, uncertainty on the Slope term is estimated around $\pm 1.5 N.m^{-3}$.

Radiation stress term

The wave radiation stress term $M_r = \frac{1}{(\bar{\eta}+h)}\frac{\partial S_{xx}}{\partial x}$ is estimated from bottom pressure wave height measurements using linear theory (Longuet-Higgins & Stewart, 1962), neglecting wave-roller effects (Buckley et al., 2015). Typical ranges of water depth, wave height, and horizontal distances of 1 ± 0.015 m, 1 ± 0.05 m, and 100 ± 0.075 m, yield uncertainty estimates on the radiation stress term around $3\,N.m^{-3}$.

Friction term

A classic quadratic law is used to compute the total bed shear stress (Feddersen et al., 2000; Buckley et al., 2016) combining the contributions of the depth-averaged current U and the wave bottom orbital velocity u_b:

$$\tau_b = \rho C_d \overline{|U + u_b|\,(U + u_b)} \tag{2}$$

where C_d is the bottom drag coefficient. This current-wave decomposition is generally valid for the thick boundary layer present in coral reefs (A. W. Pomeroy et al., 2017; Lentz et al., 2018; Sous, Dodet, et al., 2020). The depth-averaged current U in each zone is estimated from the time-averaged depth-averaged profile of cross-reef velocity measured at AQP1 weighted by the depth ratio. The horizontal component of the orbital velocity at the bottom, u_b, is estimated from the time series of instantaneous bottom pressure P_b using linear wave theory:

$$u_b = \frac{C P_b}{\rho g(\bar{\eta} + h)}, \tag{3}$$

where $C = (g(\bar{\eta} + h))^{1/2}$ is the wave celerity.

Note that (i) u_b includes all wave components, i.e. both short and infragravity waves and, (ii), the ratio u_b/U ranges here between 1.6 and 25, i.e. generally much higher than the values observed by Lentz et al. (Lentz et al., 2017), making the present dataset particularly useful to quantify the influence of waves on drag over coral reefs. Finally, the Friction term defined in Equation 1 can be directly derived from the in-situ measurements as

$$M_f = \frac{\rho}{(\bar{\eta} + h)} \overline{|U + u_b|\,(U + u_b)} \tag{4}$$

Momentum-based bottom drag coefficient

Based on the estimation of the three momentum fluxes described above, an experimental value of the bottom drag coefficient, C_d^{exp}, can be obtained from Equation 1:

$$C_d^{exp} = -\frac{M_s + M_r}{M_f} \tag{5}$$

Theoretical bottom drag coefficient

The depth-dependence of the bottom drag coefficient is furthermore assessed in the framework of the canonical turbulent logarithmic mean velocity profile (law of the wall). In the presence of large and highly variable roughness, the proper definition of a $z = 0$ datum (here the RSE) is generally not straightforward. A displacement height d is generally introduced to define the hydrodynamic origin, leading to the following formulation of the law of the wall (Kundu & Cohen, 1990):

$$\langle u(z) \rangle = \frac{U_*}{\kappa} \ln \left(\frac{z-d}{z_0} \right) \tag{6}$$

where $\langle u(z) \rangle$ is the time-averaged velocity profile at elevation z above the bed, U_* is the friction velocity, $\kappa = 0.41$ the Karman constant, and z_0 and d are the roughness and displacement heights, respectively. Depth-integration of Equation 6 leads to a theoretical expression for the drag coefficient (A. Pomeroy et al., 2012; Sous, Dodet, et al., 2020):

$$C_d^{th} = \left[\frac{\kappa}{\left(ln \left(\frac{h+\bar{\eta}-d}{z_0} \right) - 1 \right)} \right]^2 . \tag{7}$$

In the following, both the experimental momentum-derived C_d^{exp}, and log-derived theoretical C_d^{th}, will be considered and compared. To be valid, Equation 7 requires the full development of the boundary layer throughout the water column, meaning that (i) the velocity defect correction (Coles, 1956) can be neglected and (ii) the roughness-to-depth ratio remains weak otherwise in-canopy flow should be considered (Rosman & Hench, 2011). This latter constraint is further discussed in Section 4.

3 Results

3.1 Overview

Figure 1 shows time series of wave heights across the barrier (Fig. 1D), mean water levels (MWL, Fig. 1E) and cross-reef current and transport (Fig. 1F). The wave climate is representative of the south-west coast conditions, with mean significant wave height of $1.9\,m$ and mean peak period about $13.5\,s$. The mean wave direction hits the forereef with a 17^o southward incidence. With expected further refraction across the forereef (Sous et al., 2019), the overall wave forcing of the reef barrier is mainly reef normal. The swell attenuation is very effective, with less than 25% and 3% of the forereef wave height remaining at OSS2 and OSS6 stations, respectively. The MWL time series (Fig. 1E) shows the typical microtidal regime at Maupiti, with tide amplitude between 5 and 10cm. In most cases, the reef crest MWL (OSS2 in Fig. 1E) is higher than further shoreward on the backreef, mostly due to wave setup. This trend weakens during the most energetic event, due to the larger extension of the surf zone. The top of the reef crest colony has been measured at 5.8 cm, indicating that the reef is submerged during low water periods, by less than, on average, 15cm. For the following analysis of depth-averaged momentum fluxes, two specific periods are selected (grey patches in Figures 1D, E, F) where the reef crest submergence is at least 20 cm, allowing for a well-established cross-reef dynamics, with a deviation from the cross-reef direction lower than 15^o. Cross-reef current and transport (Fig. 1E) are clearly driven by incoming wave energy (Sous et al., 2017; Sous, Dodet, et al., 2020): the larger the waves, the stronger the cross-barrier barotropic pressure gradient, thus, the stronger the current is.

3.2 Depth-averaged momentum fluxes

Figure 2 shows Radiation and Slope terms relative to Friction, for the four selected zones. Two experimental constant-value C_d are displayed for each zone: $C_d^{exp,f}$,

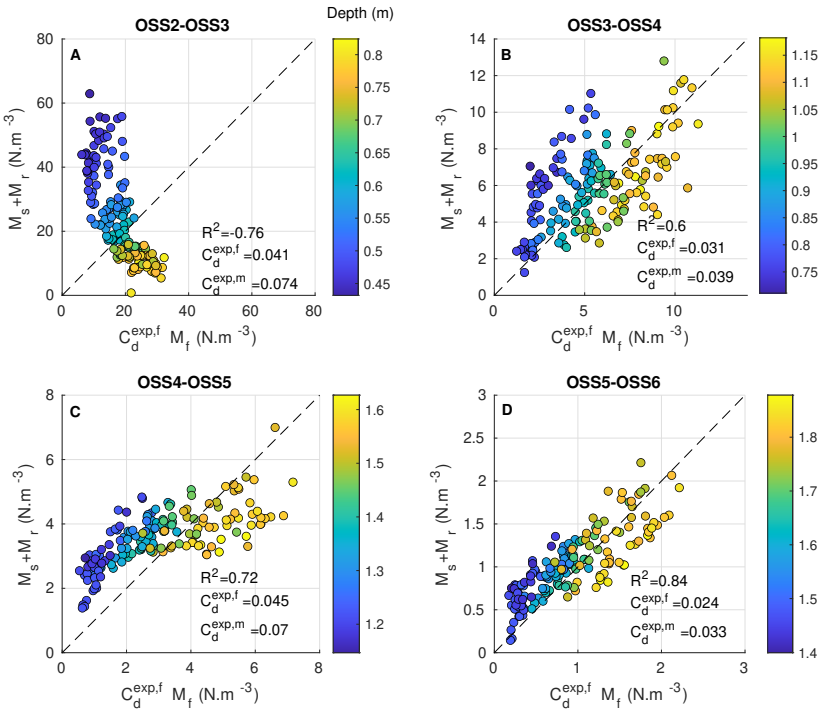

Figure 2. Cross-shore depth-averaged momentum fluxes for the four selected zone (RC: Reef Crest, BrA: Backreef A, BrB: Backreef B, BrC: Backreef C). The local depth is given in color levels. The value $C_d^{exp,f}$ refers to the value obtained from the linear fit of the $M_s + M_r$ vs M_f relationship, while $C_d^{exp,m}$ refers to the time-averaged value of all the individual estimates.

which refers to the value obtained from the linear fit of the $M_s + M_r$ vs M_f relationship, and $C_d^{exp,m}$ which refers to the averaged value over all the individual estimates. The constant C_d approach results in an overall unsatisfactory representation of the observed physics. The quality of the regression ($R^2 = 0.84$) is acceptable for the deeper part of the backreef (BrC, Fig. 2D) but R^2 strongly decreases when moving offshore. The bottom drag coefficients obtained for the three backreef zones show significant variations, with no clear trend for both $C_d^{exp,f}$ and $C_d^{exp,m}$. In addition, strong differences appear between C_d estimates obtained with linear fit and global average methods. A well marked depth effect is observed, as indicated by color levels of zone-averaged depths in Figure 2.

Further insight is gained by plotting the time-varying bottom drag coefficient, calculated using Eqn. 5, versus the local depth (see Figure 3A). For each zone, a straightforward depth-dependence is observed. The bottom drag coefficient strongly increases in shallow depth, following previous observations (McDonald et al., 2006; A. Pomeroy et al., 2012; Lentz et al., 2017, 2018; Sous, Dodet, et al., 2020). In Figure 3A, the depth-dependent C_d at each zone is compared with the theoretical predictions of the log-layer C_d^{th} formulation given in Equation 7, z_0 and d being used as least-square fitting parameters. A satisfactory agreement is obtained, with a good representation of the observed depth-dependent C_d for all zones. In addition to the full-data model fitting presented in Figure 3, a bootstrap analysis over 100 40-item subsamples randomly selected from the initial 140-item dataset was carried out to estimate uncertainties on d and z_0. This leads to mean values of 0.35, 0.52, 0.93

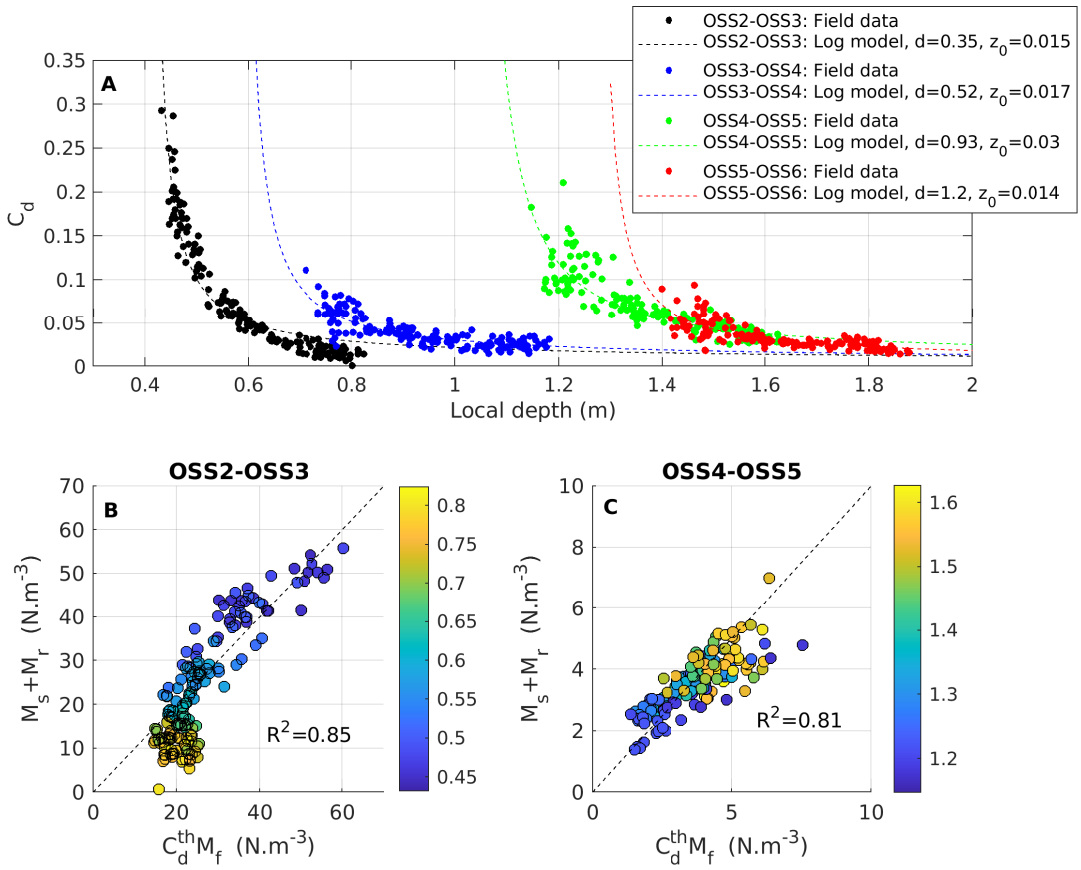

Figure 3. A: Depth-dependence of the bottom drag coefficient for the four zones. Circles and dashed lines correspond to field measurements and log-C_d fitted formulations, respectively. For each zone, the log-C_d fit provides the displacement d and roughness z_0 heights (in m). B and C: Cross-shore depth-averaged momentum balance with the log-derived bottom drag coefficient for Reef Crest (RC) and BackReef B (BrB) zones, respectively. The local depth is given in color levels.

and 1.2 m for d and 0.015, 0.017, 0.03 and 0.14 m for z_0 for RC, BrA, BrB and BrC, respectively, and standard deviations of 0.0011, 0.0026, 0.003 and 0.0018 m for d and 0.011, 0.059, 0.042 and 0.054 m for z_0 for RC, BrA, BrB and BrC, respectively. Various sub-sample sizes (ranging from 20 to 50) were tested, with no clear influence on the results. The overall trend is that d increases from the reef crest to the backreef while the roughness height z_0 is more constant throughout. The implementation of the log-C_d clearly improves the balance between the depth-averaged momentum terms compared to the constant approach (compare Fig. 3B and C with Fig. 2A and C). Linear determination coefficients between $M_s + M_r$ and $C_d^{th} M_f$ are 0.85, 0.82, 0.81 and 0.87 for RC, BrA, BrB and BrC, respectively, indicating a much better closure of the momentum balance than with the constant C_d approach used in Figure 2.

4 Discussion

The present study aims to take advantage of a specific barrier reef site, selected for its well-structured roughness variability, to provide new insights on friction processes

and bottom drag coefficients in coral reef environments. The strategy followed here is to infer the drag coefficient from a careful examination of the governing momentum equation over selected zones of the barrier (Lentz et al., 2017; Sous, Dodet, et al., 2020). This bulk approach, i.e. deducing the bottom drag coefficient from momentum balance, allowed us to spatially integrate the bottom drag effect over a large area (Reidenbach et al., 2006) and to minimize the potential local effects which may explain the discrepancy often observed between friction estimates obtained with different methods at the same site (Dewey & Crawford, 1988; Sanford & Lien, 1999; Stahr & Sanford, 1999; Johnson et al., 1994; Lu et al., 2000; Luznik et al., 2007). The overall good balance between momentum fluxes validates the depth-effect parameterization for C_d. In addition, it enforces the relevancy of the simple mean current - wave component splitting used in the bed shear stress calculation, as suggested by (Wright & Thompson, 1983) and later used by (Lentz et al., 2018; Sous, Dodet, et al., 2020) in the coral reef context.

Our depth-effect parameterization is based on the framework provided by the log-layer boundary layer theory. The full development of such a constant flux layer requires that the typical roughness elevation remains small compared to the total water depth, while high roughness-to-depth ratio conditions should be addressed by canopy approaches (Rosman & Hench, 2011). The small roughness-to-depth ratio hypothesis is most likely violated in a number of our observations, where coral mounds can protrude above half of the water column, leaving too little space for a fully turbulent log-layer to develop. This should explain why unrealistically high values of d are reached when fitting the log-layer C_d model to the observations. The exact threshold of roughness-to-depth ratio required to reach the full development of a log layer remains an open question in such complex environment and would require a comprehensive space and time averaging of velocity profiles across the considered area. One notes however that the proposed log-based parameterization of C_d remains quite robust in describing the C_d depth-dependency. The question arises then on the possible connection between the fitting parameters of the model, inferred from purely hydrodynamical observations, and the coral reef topography.

Understanding the relationship between the geometric structure of the bottom and the hydrodynamic parameters remains an open challenge. For simple geometrical structures, a "discrete" approach can be used to connect frictional height with a combination of real roughness element scales such as height, width, and spacing. Well-known scalings for log-layer roughness height are for instance $z_0 = h_r/30$ (Bowden, 1978), where h_r is grain diameter for sandy beds, or $27.7H^2/L$ for ripple beds (Grant & Madsen, 1982) where H and L are the ripple height and width. More complex geometries, observed on most rock and reef seafloors, are often treated similarly by assuming the existence of a single representative hydrodynamic roughness height (Schlichting & Gersten, 2016). The question arises then on the connection of the roughness height with the real geometric structure of the seabed. Roughness heights being spatially-integrative parameters, the discrete estimators may need to be complemented by a "continuous" approach of seabed complexity through statistical moments and moment functions (Flack & Schultz, 2010; Stewart et al., 2019; Davis et al., 2020). Only recently has there been progress in the in-situ fine spectral description of living coral reef topography over a relevant range of length-scales (Nunes & Pawlak, 2008; Jaramillo & Pawlak, 2011; Duvall et al., 2019; Rogers et al., 2018; Sous, Dodet, et al., 2020). A proper assessment of friction processes over complex seabeds will require a long-term research effort, combining field and laboratory databases, such as the exploration of the friction processes over laboratory synthetic self-affine surfaces (surfaces including a spectral power law dependence on wavenumber (Turcotte & Brown, 1993)) carried out by Stewart et al. (2019). Our depth-effect parameterization is based on two fitting parameters, z_0 and d. The former showed no clear connection with the seabed statistical features derived by Sous et al. (2020). The latter can be connected to the standard elevation of the seabed σ (see Figure 4). Considering the 10-th percentile

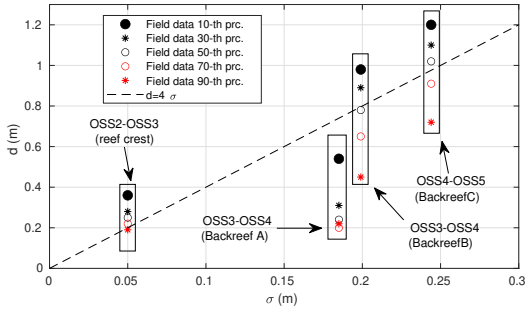

Figure 4. Displacement height d vs bed elevation standard deviation σ for the four selected zones. The dashed line $d = 4\sigma$ is given as statistical reference.

RSE (black dots in Fig. 4), an overall linear tendency is observed, revealing the connection between the topography statistics and the displacement height ($d = 4\sigma$ is given in Fig. 4 as a statistical reference). It is however worth mentioning that the BrA zone displays a lower displacement height than the overall trend, i.e. the standard deviation of bed elevation is not a comprehensive predictor of d. While showing nearly similar standard deviation of bed elevation as the BrB zone, the BrA zone displays a much higher negative skewness of the coral elevation distribution. The lower displacement height for BrA, associated with a lower friction, may be attributed to an evolution of the boundary layer structure, closer to a δ-type roughness functioning for BrA, with skimming flow over colony crest and stable circulation cells in troughs, and more similar to a k-type roughness functioning for BrB, with more unstable eddies. While a comprehensive characterization of the 3D flow structure remains to be done, this observation indicates that, even if many reefs can be *hydrodynamically* associated to $k - \delta$-type roughness (i.e. with lee eddies and flow reattachment between roughness elements) (Rogers et al., 2018), the bottom drag remains very sensitive to the actual colony geometrical structure.

Another important discussion point is the distinction between bathymetry and roughness. Any flow feels the bed effect as a whole, therefore the need to distinguish between these scales mostly arises from the requirements of numerical models, in particular the horizontal resolution. In essence, bathymetry is resolved and roughness is parameterized. The effective spatial resolution is determined by both the numerical strategy (computational effort) and the resolution of the available bed topography measurements. Apart from specific cases, the horizontal resolution in nearshore and coastal models usually ranges from a few meters to a few dozen meters. This indicates that a large range of the living reef topographic complexity cannot be explicitly resolved and must be parameterized as roughness. In addition, the definition of the bathymetry reference datum in turn defines the water depth, and is therefore of primary importance to assess the depth-effect on bottom friction. The present analysis of the momentum balance has been based on the 10-th percentile of bed elevation. A sensitivity analysis has been performed with additional RSE estimations using the 30, 50, 70 and 90-th percentiles, i.e. gradually rising the bathymetry. The quality of the momentum balance regression remained satisfactory in any case. The displacement height d obtained from the log-fitted-C_d showed an overall decrease with increasing bathymetry (see Fig. 4), while no clear trend was observed on the roughness height z_0. A lower displacement height for BrA zone was found to be systematically lower (Figure 4). These observations emphasize the need to carefully define the bathymetric referential in attempts to assess or to parameterize friction over multi-scale rough seabeds.

5 Summary and conclusion

Results from a 3 week experiment on the Maupiti south-west barrier reef demonstrate that, even at the scale of a single barrier reef, C_d is strongly variable in time and space. We extend on previous observations (McDonald et al., 2006; Lentz et al., 2017) of C_d's strong dependence on both local depth and reef topographical structure, to a wave-exposed environment with higher roughness values and large C_d. For a given site, C_d ranges by one order of magnitude due to the range of depths observed. The dependency of the bottom drag coefficient on both water depth and reef structure can be convincingly represented by a log depth-dependent C_d formulation. At the higher end of the depth range observed here, the bottom drag coefficient tends to a nearly depth-independent value ranging 0.02 and 0.035.

In addition to depth, the geometrical structure of the coral colony affects the bottom drag coefficient. The connection between reef geometry and its hydrodynamical function can be identified through the roughly linear relationship observed between the standard deviation of the reef elevation and the displacement height used in the log depth-dependent C_d formulation. Third-order statistical moment (skewness) of bed elevation is also observed to affect bottom drag, likely associated with an effect on the near-bed flow structure. The analysis raises the need for more comprehensive in-situ data connecting hydrodynamic friction parameters and structural complexity of reef colony.

6 Open Research

The presented data can be freely available at https://doi.org/10.34930/9db3bec4-0bbf-4531-8864-f100c4b8eced

References

Bowden, K. F. (1978). Physical problems of the benthic boundary layer. *Geophys. Surveys*, *3*, 255-296.

Buckley, M. L., Lowe, R. J., Hansen, J. E., & Van Dongeren, A. R. (2015). Dynamics of wave setup over a steeply sloping fringing reef. *Journal of Physical Oceanography*, *45*(12), 3005–3023.

Buckley, M. L., Lowe, R. J., Hansen, J. E., & Van Dongeren, A. R. (2016). Wave setup over a fringing reef with large bottom roughness. *Journal of Physical Oceanography*, *46*(8), 2317–2333.

Chevalier, C., Sous, D., Devenon, J.-L., Pagano, M., Rougier, G., & Blanchot, J. (2015). Impact of cross-reef water fluxes on lagoon dynamics: a simple parameterization for coral lagoon circulation model, with application to the ouano lagoon, new caledonia. *Ocean Dynamics*, *DOI: 10.1007/s10236-015-0879-x*, 1509-1534.

Coles, D. (1956). The law of the wake in the turbulent boundary layer. *Journal of Fluid Mechanics*, *1*(2), 191–226.

Davis, K. A., & Monismith, S. G. (2011). The modification of bottom boundary layer turbulence and mixing by internal waves shoaling on a barrier reef. *Journal of Physical Oceanography*, *41*(11), 2223–2241.

Davis, K. A., Pawlak, G., & Monismith, S. G. (2020). Turbulence and coral reefs. *Annual Review of Marine Science*, *13*.

Dewey, R. K., & Crawford, W. R. (1988). Bottom stress estimates from vertical dissipation rate profiles on the continental shelf. *J. Phys. Oceanogr.*, *18(8)*, 1167–1177.

Duvall, M. S., Hench, J. L., & Rosman, J. H. (2019). Collapsing complexity: quantifying multi-scale properties of reef topography. *Journal of Geophysical Research: Oceans*, *124*, 5021–5038.

Feddersen, F., Guza, R., Elgar, S., & Herbers, T. (2000). Velocity moments in alongshore bottom stress parameterizations. *Journal of Geophysical Research: Oceans*, *105*(C4), 8673–8686.

Flack, K. A., & Schultz, M. P. (2010). Review of hydraulic roughness scales in the fully rough regime. *Journal of Fluids Engineering*, *132*(4).

Gourlay, M. (1996). Wave set-up on coral reefs. 1. set-up and wave-generated flow on an idealised two dimensional horizontal reef. *Coastal Engineering*, *27*(3), 161–193.

Gourlay, M. R., & Colleter, G. (2005). Wave-generated flow on coral reefs—an analysis for two-dimensional horizontal reef-tops with steep faces. *Coastal Engineering*, *52*(4), 353–387.

Grant, W. D., & Madsen, O. S. (1982). Movable bed roughness in unsteady oscillatory flow. *Journal of Geophysical Research: Oceans*, *87*(C1), 469–481.

Hearn, C. J. (1999). Wave-breaking hydrodynamics within coral reef systems and the effect of changing relative sea level. *Journal of Geophysical Research: Oceans (1978–2012)*, *104*(C12), 30007–30019.

Hench, J. L., & Rosman, J. H. (2013). Observations of spatial flow patterns at the coral colony scale on a shallow reef flat. *Journal of Geophysical Research: Oceans*, *118*(3), 1142–1156.

Jaramillo, S., & Pawlak, G. (2011). Auv-based bed roughness mapping over a tropical reef. *Coral Reefs*, *30*(1), 11–23.

Jiménez, J. (2004). Turbulent flows over rough walls. *Annu. Rev. Fluid Mech.*, *36*, 173–196.

Johnson, G. C., Lueck, R. G., & Sanford, T. B. (1994). Stress on the mediterranean outflow plume: Part ii. turbulent dissipation and shear measurements. *J. Phys. Oceanogr.*, *24*, 2084–2092.

Kundu, P., & Cohen, L. (1990). Fluid mechanics. *Academic, Calif*.

Lentz, S., Churchill, J. H., & Davis, K. A. (2018). Coral reef drag coefficients—surface gravity wave enhancement. *Journal of Physical Oceanography*, *48*(7), 1555–1566.

Lentz, S., Davis, K., Churchill, J., & DeCarlo, T. (2017). Coral reef drag coefficients–water depth dependence. *Journal of Physical Oceanography*, *47*(5), 1061–1075.

Leonardi, S., Orlandi, P., & Antonia, R. A. (2007). Properties of d-and k-type roughness in a turbulent channel flow. *Physics of fluids*, *19*(12), 125101.

Longuet-Higgins, M. S., & Stewart, R. (1962). Radiation stress and mass transport in gravity waves, with application to 'surf beats'. *Journal of Fluid Mechanics*, *13*(4), 481–504.

Lowe, R. J., Falter, J. L., Bandet, M. D., Pawlak, G., Atkinson, M. J., Monismith, S. G., & Koseff, J. R. (2005). Spectral wave dissipation over a barrier reef. *Journal of Geophysical Research: Oceans (1978–2012)*, *110*(C4).

Lu, Y., Lueck, R. G., & Huang, D. (2000). Turbulence characteristics in a tidal channel. *J. Phys. Oceanogr.*, *30*, 855-867.

Luznik, L., Gurka, R., Smith, W. A. M. N., Zhu, W., Katz, J., & Osborn, T. R. (2007). Distribution of energy spectra, reynolds stresses, turbulence production and dissipation in a tidally driven bottom boundary layer. *J. Phys. Oceanogr.*, *37*, 1527-1550.

McDonald, C., Koseff, J., & Monismith, S. (2006). Effects of the depth to coral height ratio on drag coefficients for unidirectional flow over coral. *Limnology and oceanography*, *51*(3), 1294–1301.

Monismith, S. G. (2007). Hydrodynamics of coral reefs. *Annu. Rev. Fluid Mech.*, *39*, 37–55.

Monismith, S. G., Rogers, J. S., Koweek, D., & Dunbar, R. B. (2015). Frictional wave dissipation on a remarkably rough reef. *Geophysical Research Letters*, *42*(10), 4063–4071.

Nunes, V., & Pawlak, G. (2008). Observations of bed roughness of a coral reef. *Journal of Coastal Research*(24), 39–50.

Pomeroy, A., Lowe, R., Symonds, G., Van Dongeren, A., & Moore, C. (2012). The dynamics of infragravity wave transformation over a fringing reef. *Journal of Geophysical Research: Oceans (1978–2012)*, *117*(C11).

Pomeroy, A. W., Lowe, R. J., Ghisalberti, M., Storlazzi, C., Symonds, G., & Roelvink, D. (2017). Sediment transport in the presence of large reef bottom roughness. *Journal of Geophysical Research: Oceans*, *122*(2), 1347–1368.

Reid, E., Lentz, S., DeCarlo, T., Cohen, A., & Davis, K. (2020). Physical processes determine spatial structure in water temperature and residence time on a wide reef flat. *Journal of Geophysical Research: Oceans*, *125*(12), e2020JC016543.

Reidenbach, M. A., Monismith, S. G., Koseff, J. R., Yahel, G., & Genin, A. (2006). Boundary layer turbulence and flow structure over a fringing coral reef. *Limnology and Oceanography*, *51*(5), 1956.

Rogers, J. S., Maticka, S. A., Chirayath, V., Woodson, C. B., Alonso, J. J., & Monismith, S. G. (2018). Connecting flow over complex terrain to hydrodynamic roughness on a coral reef. *Journal of Physical Oceanography*, *48*(7), 1567–1587.

Rosman, J. H., & Hench, J. L. (2011). A framework for understanding drag parameterizations for coral reefs. *Journal of Geophysical Research: Oceans*, *116*(C8).

Sanford, T. B., & Lien, R. C. (1999). Turbulent properties in a homogeneous tidal bottom boundary layer. *J. Geophys. Res*, *104 (C1)*, 1245–1257.

Schlichting, H., & Gersten, K. (2016). *Boundary-layer theory*. Springer.

Sous, D., Bouchette, F., Doerflinger, E., Meulé, S., Certain, R., Toulemonde, G., ... Salvat, B. (2020). On the small-scale fractal geometrical structure of a living coral reef barrier. *Earth Surface Processes and Landforms*, *45*(12), 3042–3054.

Sous, D., Chevalier, C., Devenon, J.-L., Blanchot, J., & Pagano, M. (2017). Circulation patterns in a channel reef-lagoon system, ouano lagoon, new caledonia. *Estuarine, Coastal and Shelf Science*, *196*, 315–330.

Sous, D., Dodet, G., Bouchette, F., & Tissier, M. (2020). Momentum balance over a barrier reef. *Journal of Geophysical Research: Oceans*, *DOI: 10.1029/2019JC015503*.

Sous, D., Tissier, M., Rey, V., Touboul, J., Bouchette, F., Devenon, J.-L., ... Aucan, J. (2019). Wave transformation over a barrier reef. *Continental Shelf Research*, *184*, 66–80.

Stahr, F. R., & Sanford, T. B. (1999). Transport and bottom boundary layer observations of the north atlantic deep western boundary current at the blake outer ridge. *Deep Sea Res.*, *46*, 205–243.

Stewart, M. T., Cameron, S. M., Nikora, V. I., Zampiron, A., & Marusic, I. (2019). Hydraulic resistance in open-channel flows over self-affine rough beds. *Journal of Hydraulic Research*, *57*(2), 183–196.

Symonds, G., Black, K. P., & Young, I. R. (1995). Wave-driven flow over shallow reefs. *Journal of Geophysical Research: Oceans (1978–2012)*, *100*(C2), 2639–2648.

Turcotte, D. L., & Brown, S. R. (1993). Fractals and chaos in geology and geophysics. *Physics Today*, *46*(5), 68.

Wooding, R., Bradley, E. F., & Marshall, J. (1973). Drag due to regular arrays of roughness elements of varying geometry. *Boundary-Layer Meteorology*, *5*(3), 285–308.

Wright, D. G., & Thompson, K. R. (1983). Time-averaged forms of the nonlinear stress law. *Journal of Physical Oceanography*, *13*(2), 341–345.